

Detecting stratigraphic discontinuities using time-frequency seismic phase residues

Marcílio Castro de Matos¹, Oswaldo Davogustto², Kui Zhang², and Kurt J. Marfurt²

ABSTRACT

Spectral decomposition is a proven, powerful means of identifying strong amplitude anomalies at specific frequencies that are otherwise buried in the broadband response. Most publications focus on using spectral magnitude instead of phase components to identify lateral changes in stratigraphy, wavefield attenuation from the quality factor Q , and unconformities between geologic formations. Although seismic acquisition and processing preserve phase very well, little has been published about interpreting the phase components resulting from spectral decomposition. Morlet complex wavelet transform phase residues can improve seismic spectral decomposition interpretation by detecting the phase discontinuities in the joint time-frequency spectral phase component. Phase singularities can be associated with geologic features, and work with phase residues can improve interpretation of the Anadarko basin Red Fork channels of Oklahoma, U.S.A.

INTRODUCTION

Seismic interpretation is based on amplitude variation with time and space. Usually, interpreters look for relatively coherent seismic amplitudes that represent impedance contrasts associated with geologic boundaries (Henry, 2004). In this paper, we assume that seismic amplitudes can be modeled using a simple convolutional operation between the reflection coefficient series that represents the geology and the seismic wavelet that represents an impulsive seismic source after passing through the earth filter.

Stratigraphic variations from changes in the depositional systems or diagenesis (in carbonates) (Hart, 2008) generate different reflectivity coefficient series for each environment and, consequently,

different kinds of seismic waveforms. In addition to phase changes from stratigraphy, phase rotations can be introduced through seismic processing and may be further adjusted by the interpreter (Roden and Sepulveda, 1999). Some of the geology-induced phase shifts can be identified easily, such as spatial discontinuities associated with faults and incised channels; but phase shifts from condensed sections and erosional unconformities can be quite subtle. Stark (2003) shows that high gradient values of the 2D unwrapped instantaneous phase (Ghiglia and Pritt, 1998) obtained from a complex trace analysis can delineate some of these features.

We use Morlet complex continuous wavelet transform (CWT) spectral decomposition to measure phase changes as a function of frequency and show how such changes can be related to seismic stratigraphy. Beginning with a simple review of spectral decomposition, we emphasize the phase rather than the magnitude component. Next, we review some of the theory on phase unwrapping. Then, instead of attempting to unwrap the phase (a fairly difficult problem), we show how we can compute a phase residue, i.e., anomalies in the phase spectra. Finally, we compare the phase residues computed from a seismic data volume acquired over the Anadarko basin, Oklahoma, U.S.A., with well-log data to validate the resolution of thin sands that fall at the limit of seismic resolution.

Spectral decomposition: Generating time-frequency amplitude and phase spectra

Partyka et al. (1999) first showed how the seismic spectral response from a short time window can be used to map lateral changes in acoustic properties and thickness of stratigraphic layers. Since then, spectral decomposition has become a widely accepted interpretation tool when applied to clastic sediments and has been applied to reservoir characterization (Matos et al., 2005; Liu and Marfurt, 2007), hydrocarbon detection (Castagna et al., 2003), and stratigraphic analysis (Hall and Trouillot, 2004). Most spectral decomposition applications are based on the magnitude component of the joint time-frequency spectrum. Although some of these

Manuscript received by the Editor 25 November 2009; revised manuscript received 1 October 2010; published online 24 March 2011.

¹Formerly at University of Oklahoma, School of Geology and Geophysics, Norman, Oklahoma, U.S.A.; presently an independent consultant. E-mail: marcilio@matos.eng.br.

²University of Oklahoma, School of Geology and Geophysics, Norman, Oklahoma, U.S.A. E-mail: dellpi@ou.edu; kui.zhang-1@ou.edu; kmarfurt@ou.edu.
© 2011 Society of Exploration Geophysicists. All rights reserved.

techniques are quadratic-energy based, such as the Wigner-Ville distribution, and do not generate phase information, the short-window discrete Fourier transform, wavelet transform, and matching pursuit algorithms all produce complex spectra that can be represented by magnitude and phase components. Phase spectra respond to lateral discontinuities and have been used successfully to delineate faults. However, to our knowledge, very little has been published on the spectral phase response resulting from stratigraphy or on mapping spectral phase discontinuities.

Following the method of Partyka et al. (1999), we start by evaluating the phase shift introduced by bed-thickness changes. A review of basic math helps us understand the effects of thin-bed tuning discussed in the wedge model shown in Figure 1. We define the thickness of the wedge at any point along the horizontal axis as ΔT . Then we can interpret the reflector from the top of the wedge as having a negative polarity and a phase advance of $\Delta T/2$. We can also interpret the reflector from the bottom of the wedge as having a positive polarity and a phase delay of $\Delta T/2$. If we divide the composite reflection response by ΔT , we obtain the finite-difference approximation to the derivative:

$$\frac{\partial u}{\partial T} \equiv \lim_{\Delta T \rightarrow 0} \frac{u(t + \frac{\Delta T}{2}) - u(t - \frac{\Delta T}{2})}{\Delta T} \quad (1)$$

or

$$\lim_{\Delta T \rightarrow 0} u\left(t + \frac{\Delta T}{2}\right) - u\left(t - \frac{\Delta T}{2}\right) = \Delta T \frac{\partial u}{\partial T}. \quad (2)$$

Thus, for small thicknesses, the composite response will be the derivative of the original seismic wavelet $u(t)$ times the value of the thickness ΔT . Widess (1973) uses a version of equation 2 to estimate thin-bed thickness straight from the seismic trace $u(t)$. We recall that if the complex Fourier transform of $u(t)$ is $U(\omega)$, where ω is the temporal frequency in radians/second, then the Fourier transform (complex spectrum) of the derivative du/dt is $i\omega U(\omega)$, such that for a very thin bed the phase is rotated by 90° and the amplitude spectrum is increased proportional to the frequency ω .

Phase is an important property of waves and is related to the delay from a reference instant of time or space. Instantaneous phase is usually calculated using the arc tangent function of a complex phasor (Taner et al., 1979), generating values that lie

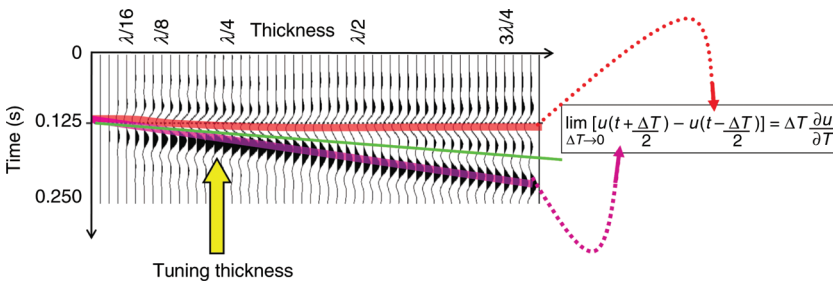


Figure 1. Seismic response of a low-impedance wedge embedded in a high-impedance matrix. The two-way traveltime thickness of the wedge is ΔT , with the green line defining its midpoint. The constructive and destructive interference of the phase-delayed positive reflection at the bottom of the wedge and phase-advanced negative reflection at the top of the wedge gives rise to the well-known tuning effect. As ΔT approaches zero, the seismic amplitude is proportional to the thickness ΔT and the derivative of the waveform, as described by Widess (1973).

between $-\pi$ and $+\pi$. However, the true phase property is not wrapped and does not suffer from mathematical discontinuities between $+\pi$ and $-\pi$. Therefore, to identify subtle phase changes, we must unwrap the phase.

A REVIEW OF PHASE UNWRAPPING

Kaplan and Ulrych (2007) report that phase unwrapping remains an important and challenging seismic data processing research topic; Ghiglia and Pritt (1998) state that phase unwrapping is also essential in processing synthetic aperture radar (SAR) images and optical fringe-pattern analysis.

Shatilo (1992) identifies several different ways to unwrap 1D seismic data. The simplest way is by using the expected continuity of the phase, allowing us to unwrap the phase using

$$\varphi_n = \psi_n + 2\pi c_n; \quad n = 0, 1, 2, \dots, N - 1, \quad (3)$$

where $c_n = \text{nint}((\psi_n - \psi_{n-1})/2\pi)$, the vector $\boldsymbol{\varphi}$ is the unwrapped phase, $\boldsymbol{\psi}$ is the wrapped phase, c indicates the number of integer cycles used in unwrapping, nint is a function that provides the nearest integer, and n indicates the sample where the phase is unwrapped. Kaplan and Ulrych (2007) propose a similar phase unwrapping computed in the complex plane.

Using the concept that the instantaneous frequency is the phase first derivative, Itoh (1982) shows that the phase can be unwrapped by integrating wrapped phase differences:

$$\begin{aligned} \varphi_n &= \varphi_0 + \sum_{m=1}^n W\{\Delta\{W\{\varphi_m\}\}\} \\ &= \varphi_0 + \sum_{m=1}^n W\{\psi_m - \psi_{m-1}\}, \end{aligned} \quad (4)$$

where W is a wrapping operator that wraps its argument value into the range $[-\pi, +\pi]$ by adding or subtracting an integer multiple of 2π radians to its argument and Δ is the difference operator.

Itoh's process is commonly applied in 2D phase unwrapping algorithms and consists of four steps:

- 1) Compute the phase differences.
- 2) Compute the wrapped phase differences.
- 3) Initialize the first unwrapped value.
- 4) Unwrap by summing the wrapped phase differences.

If the phase is not aliased or noisy, then most of the phase-unwrapping algorithms proposed are usually very effective (Matos et al., 2009).

JOINT TIME-FREQUENCY PHASE UNWRAPPING

Spectral decomposition of a seismic trace generates complex data that can be decomposed into magnitude and phase as a function of time and frequency. For each frequency f , the phase $\boldsymbol{\varphi}(t, f)$ is a measure of traveltime distance from some reference time t_0 . One might anticipate that the time-frequency phase unwrapping can be solved just by unwrapping each phase of each frequency component using the 1D technique given by equation 3

(Léonard, 2007). However, unwrapping the phase using this component-independent process will generate phase discontinuities between adjacent frequency components. This shortcoming suggests accounting for the phase relationships along the frequency as well as down the time axis to unwrap the data, thereby requiring a 2D phase-unwrapping methodology.

Basically, Itoh's (1982) equation 4 can be extended to N -dimensional signals by assuming the phase gradients are known, with the phase at point r obtained from some initial point r_0 following the path integral (Ghiglia and Pritt, 1998):

$$\varphi(r) = \int_{\Gamma} \nabla \varphi dr + \varphi(r_0), \quad (5)$$

where Γ is any path connecting points r_0 and r and where $\nabla \varphi$ is the phase gradient. Aliasing, singularities, and noise can make equation 5 highly dependent on the integration path Γ . For this reason, it is very important to know which pitfalls should be avoided in defining Γ in equation 5.

Ghiglia and Pritt (1998) provide an excellent survey of 2D phase-unwrapping techniques and show how a complex residue theorem based on vector calculus can be applied to the phase-unwrapping problem. Specifically, they choose the smallest possible path defined by a rectangular window that measures two time samples on one side and two frequency components on the other side. For every point in the wrapped phase $\varphi(t, f)$,

$$I = \frac{W\{\psi(t + \Delta t, f) - \psi(t, f)\}}{2\pi} + \frac{W\{\psi(t + \Delta t, f + \Delta f) - \psi(t + \Delta t, f)\}}{2\pi} + \frac{W\{\psi(t, f + \Delta f) - \psi(t + \Delta t, f + \Delta f)\}}{2\pi} + \frac{W\{\psi(t, f) - \psi(t, f + \Delta f)\}}{2\pi}, \quad (6)$$

where W is a wrapping operator.

If I in equation 6 is nonzero, there are inconsistent phase points, which Ghiglia and Pritt (1998) call *phase residues*. Figure 2 shows how the residue is calculated for a small portion of a typical wrapped time-frequency phase matrix.

Bone (1991) proves that the only possible values for the phase residue are 0 and ± 1 . Workers who choose to unwrap the phase try to avoid the phase residue in some manner. Our objective is much less ambitious. Instead of unwrapping the phase, we display phase-residual properties that appear in the joint time-frequency distribution as seismic attributes that can be associated with stratigraphic discontinuities and inconsistencies in seismic data quality.

Here, we use the Morlet complex CWT as a time-frequency spectral decomposition that can be defined as the convolution between the seismic trace and the time-reversed complex Morlet wavelet (Matos et al., 2007). Before we introduce the proposed seismic attributes, we review some CWT phase properties using three simple examples.

Figure 3a shows a spike signal, and Figure 3b and c illustrates its CWT magnitude and phase, respectively. The reflectivity is a simple delta function, so the CWT is a reproduction of

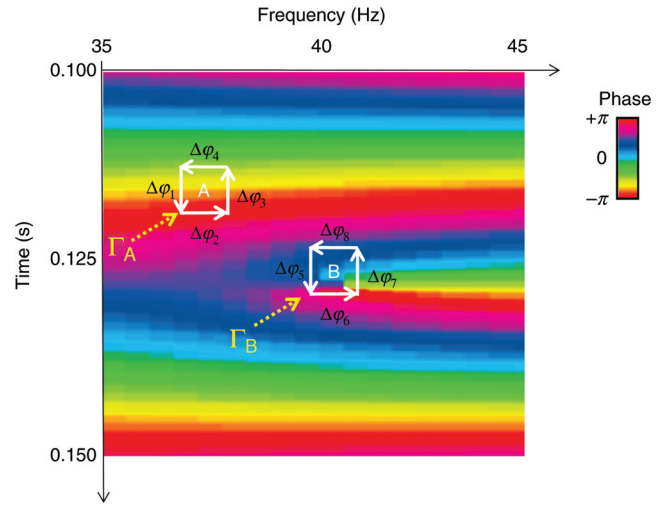


Figure 2. Computation of the phase residue r as defined by Ghiglia and Pritt (1998). The path integration Γ_A (equation 5) about point A gives $r_A = \Delta\varphi_1 + \Delta\varphi_2 + \Delta\varphi_3 + \Delta\varphi_4 = 0$. In contrast, the path integration Γ_B about point B gives $r_B = \Delta\varphi_5 + \Delta\varphi_6 + \Delta\varphi_7 + \Delta\varphi_8 = 1$, giving rise to a nonzero residue.

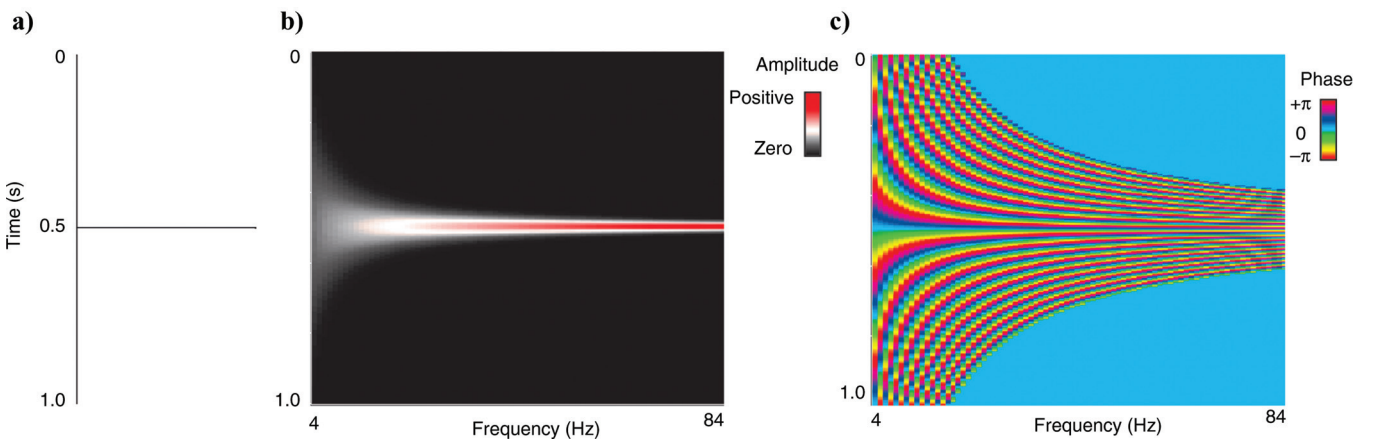


Figure 3. (a) A single-spike reflectivity series and its CWT (b) magnitude and (c) phase spectra.

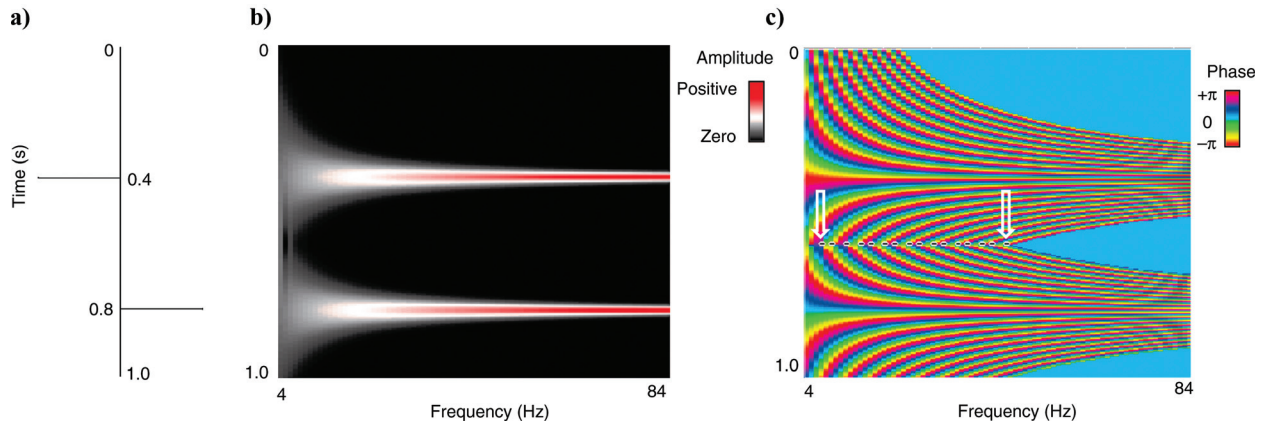


Figure 4. (a) A double-spike signal reflectivity series and its CWT, (b) magnitude, and (c) phase spectra. White arrows indicate phase residues.

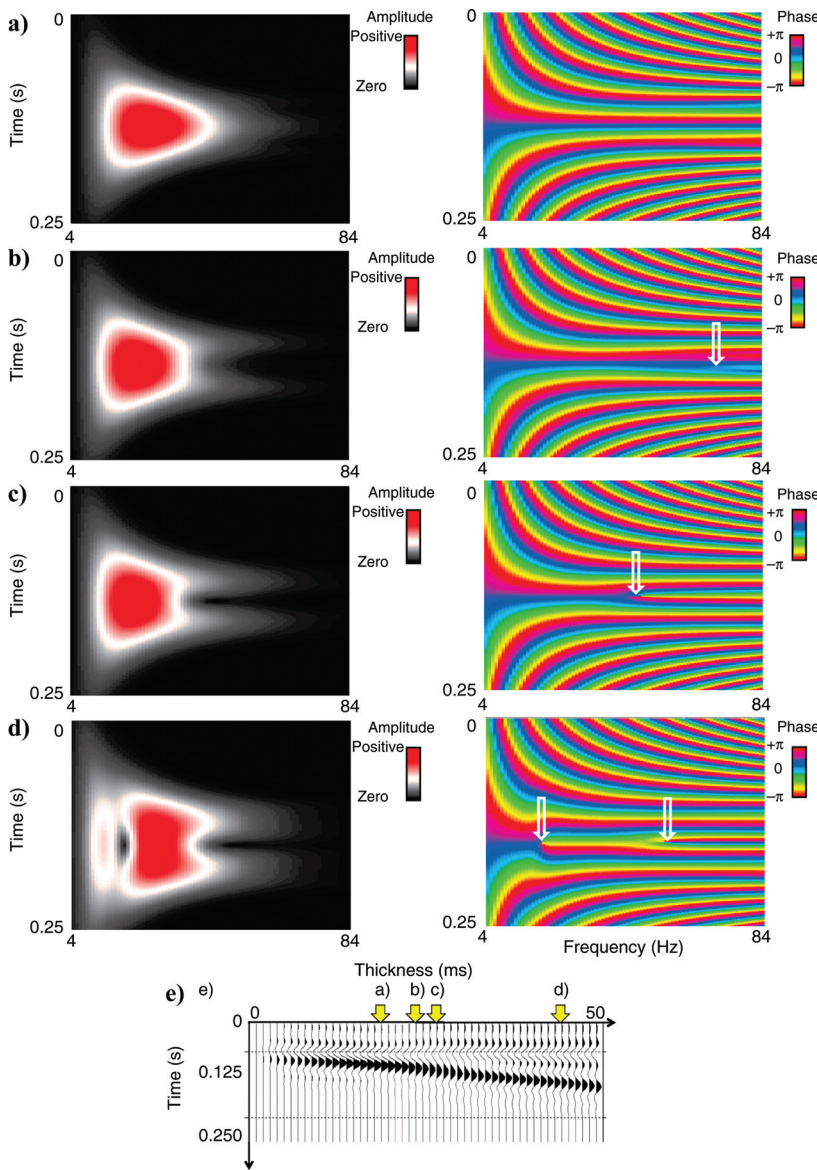


Figure 5. (a-d) CWT amplitude and phase of the four seismic traces shown in (e). White arrows indicate phase residues.

the mother wavelet at the time location of the delta function for each of the different scales. Consequently, we can clearly detect the spike by mapping the ridge of the CWT magnitude or by noting that the lines of constant CWT phase converge to the singularity point (Holschneider, 1995, p. 45). It can also be shown that discontinuities detected from the CWT unwrapped phase are associated with signal singularities (Matos et al., 2009).

When we add a second spike to the signal, as shown in Figure 4a, simulating a low-impedance reflectivity time series, we observe a similar phase and magnitude pattern at the higher frequencies. However, at the lower frequencies, residues appear in the CWT phase. Note that the residues appear between, and not at, the spikes. Note also that the CWT magnitude is very low at the residue location compared to the magnitude near the spike locations. We will use this magnitude later to determine whether a residue is significant.

Seismic data can be modeled by convolving the reflectivity with a seismic wavelet producing a filtered version of the reflectivity time series. Therefore, the CWT of a seismic trace can be interpreted as a crosscorrelation between the scaled Morlet wavelets and the seismic wavelet located at each reflectivity point where there is impedance contrast. Figure 5a and b shows the CWT magnitude and phase of a seismic trace with thickness close to zero taken from the wedge model shown in Figure 1. Compared with Figure 3, the magnitude is smeared at high frequencies, but the constant phase lines still converge to the location of the spike.

Extending the CWT analysis to representative traces of the same wedge model, Figure 5 shows the CWT amplitude and phase of representative traces and their corresponding phase residues. Contrary to the spike signal, we now note that the residues correlate to subtle phase changes in the joint time-frequency distribution. Based on these

examples, we define three new seismic attributes: the frequency where each phase residue occurs, the phase value at the residue location, and the corresponding magnitude at this frequency f and time t .

We test these attributes on a synthetic channel seismic model designed by mirroring the Figure 1 wedge model (Figure 6a). By plotting the maximum amplitude at the phase residues in Figure 6b, we can clearly see the detected channel. As expected, the proposed attributes do not detect the main reflectors and are time, or depth, shifted from them. Actually, as shown in Figure 6c, they can be associated with subtle stratigraphic interference phenomena, which we discuss in greater detail with a real data example.

Next, we add 50% random white noise to the same wedge model to verify the robustness of the attributes proposed. By using the linearity property of the CWT and knowing that the CWT of a random noise signal generates phase residues with low associated magnitude spread over the time-frequency plane (Holshneider, 1995, p. 85), we expect the phase residues can detect the same features as the previous synthetic example. Figure 7 illustrates the results and confirms that the main feature is still detected and coherent across the model.

APPLICATION

Data description

To demonstrate the value of phase residues, we use a seismic data volume that served as one of the first published applications of spectral decomposition (Peyton et al., 1998). Ten years

and hundreds of wells later in this survey, the Red Fork channels of the Anadarko basin of Oklahoma are still problematic.

The incised valleys described by Peyton et al. (1998) have undergone at least five stages of incision and fill. Suarez et al. (2008) report that the fill can comprise lag deposits, shales, coals, muddy sands, and sands. In addition to the seismically resolved incised channels, Suarez et al. (2008) note the common occurrence of invisible channels — channels seen by the drill bit and well logs but not by seismic amplitude data. From logs and check shots, using an average velocity for the Red Fork Formation of 3320 m/s (10,900 ft/s) and the dominant frequency of 50 Hz, the tuning thickness for a Red Fork channel is approximately 16 m (54 ft). The average thickness for the producing zones is 19 m (62 ft), with the maximum of the Red Fork Formation being 63 m (206 ft). Although the top and bottom of the Red Fork interval can be resolved seismically, the internal reservoir facies often fall below seismic resolution.

We selected 15 wells that fall within the survey that contained gamma-ray and self-potential (SP) curves to calibrate our phase-residue seismic anomalies. Figure 8 shows a representative synthetic seismogram used to tie the well and seismic data, and Figure 9 illustrates its CWT amplitude and phase and residues. White arrows indicate CWT phase residues associated with the Skinner horizon.

Interpretation

We applied the Morlet CWT to the seismic data volume, computed the proposed phase-residue seismic attributes, and overlaid

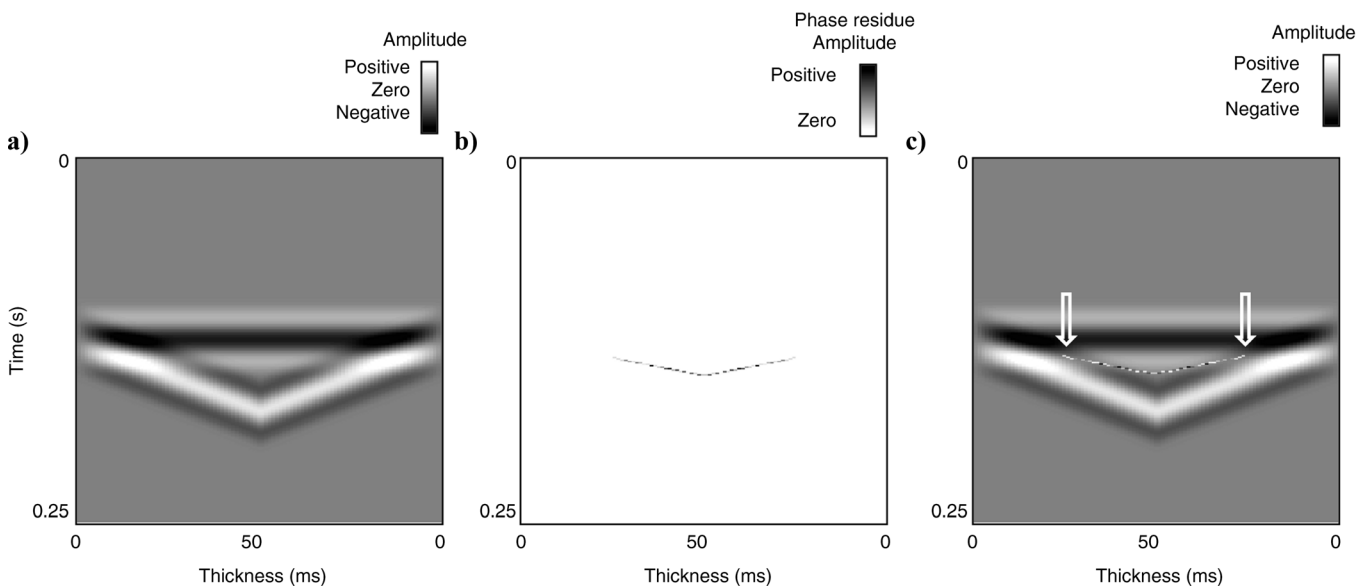


Figure 6. (a) Channel model generated by reflecting the wedge model shown in Figure 1 about the origin. (b) Phase residue modulated by the magnitude shows the channel interference pattern. (c) Seismic channel model corendered with CWT phase residue attribute. The arrows indicate the subtle stratigraphic interference phenomena detected by the proposed attribute.

the results against the gamma-ray well-log response, which allowed us to correlate phase-residue anomalies with vertical changes in lithology. Figure 10 shows the location of the composite seismic lines and the locations of the 15 wells used in the interpretation.

Examining composite line AA' (Figure 11) where we corender the seismic amplitude, the phase residues, and the gamma-ray logs, we recognize a correlation of the sand signatures in the gamma-ray logs with lineaments in the phase residue. The phase-

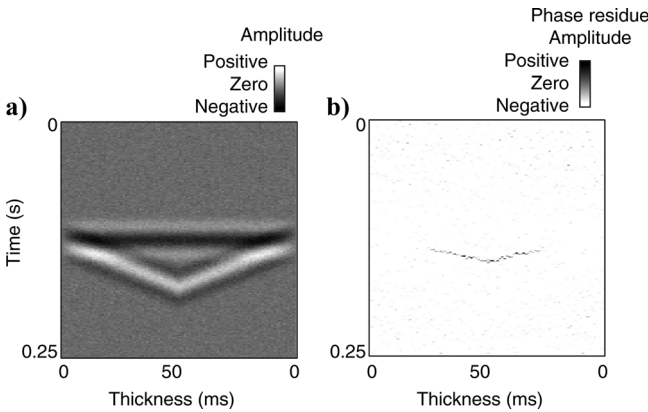


Figure 7. (a) The same channel model shown in Figure 6 contaminated by band-limited noise, giving rise to a 50% signal-to-noise ratio. (b) Phase residue modulated by the magnitude shows the channel interference pattern.

residue amplitude and frequency, blended using a 2D color map (Guo et al., 2008), allow us to interpolate these thin sands between the points of sparse well information. These sands are not apparent in the seismic amplitude data because of the limited vertical resolution. Composite line BB' (Figure 12) shows similar good correlation between the phase residue and the gamma-ray log, which we interpret to be a sand pinch-out.

In composite line CC' (Figure 13), tuning effects smear key features in the seismic amplitude data that are better defined by the phase residue. A key feature in well Z4 is a coarsening upsection that correlates with a channel feature in composite line BB' . This

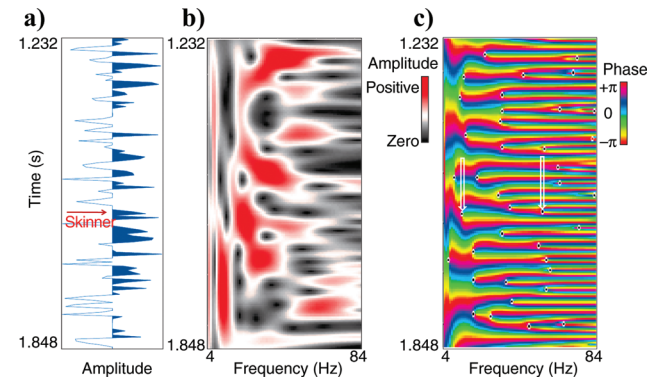


Figure 9. (a) Synthetic seismogram and its CWT (b) magnitude and (c) phase. Phase residues are indicated by black dots in (c); white arrows indicate phase residues close to the Skinner top.

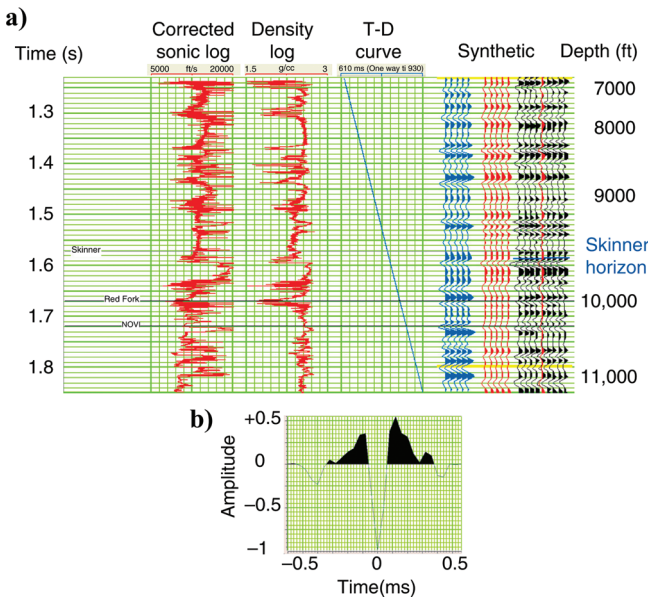


Figure 8. Synthetic seismogram for well Z5 that falls within a survey acquired in the Anadarko basin. (a) The synthetic trace shown in blue and (b) the wavelet used for the synthetic generation and the seismic well tie, giving a correlation coefficient of $R = 0.75$ for the analysis window. The sonic was corrected using a checkshot survey for the area. The wavelet was extracted using a neighborhood capture option of 30 offset ranges from the interval of 1.5–1.8 s and a full wavelet extraction.

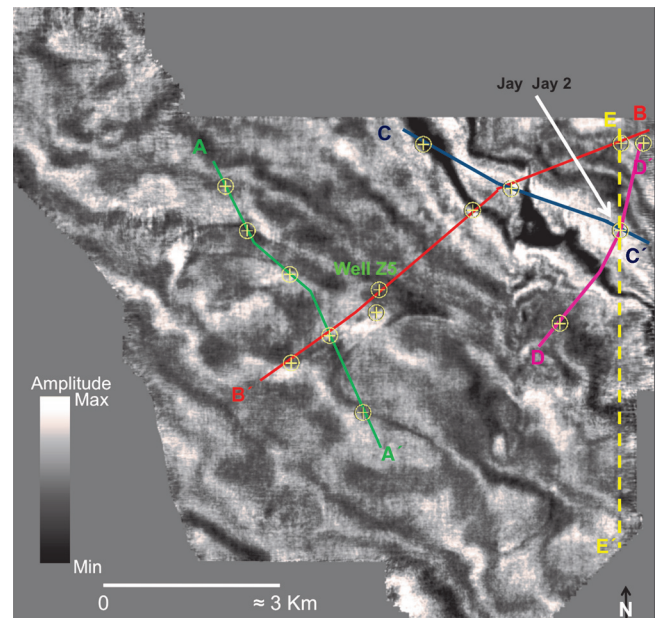


Figure 10. Phantom horizon slice 80 ms below the Skinner through the seismic amplitude volume, indicating lines AA', BB', CC', DD', and EE' through key wells.

feature is also identified in composite lines DD', EE', and Figure 16b (orange arrow). Figures 13–15 display vertical sections crossing well Jay Jay 2, with key features defined by the phase residue attribute. Peyton et al. (1998) and Suarez et al. (2008) give special importance to this well, which produces from a stage III channel sand of 15 m (50 ft) but was not imaged as a result of the moderate seismic data quality.

Figure 16a and b shows phantom horizons 80 ms below the Skinner horizon through coherence and phase-residue attributes corendered with energy-ratio similarity, respectively. Note on the vertical seismic slice that coherence (computed using a ± 20 -ms analysis window) does not have the same vertical resolution as the phase residue. Blended images of energy-ratio similarity (coherence) and phase-residue attributes (Figure

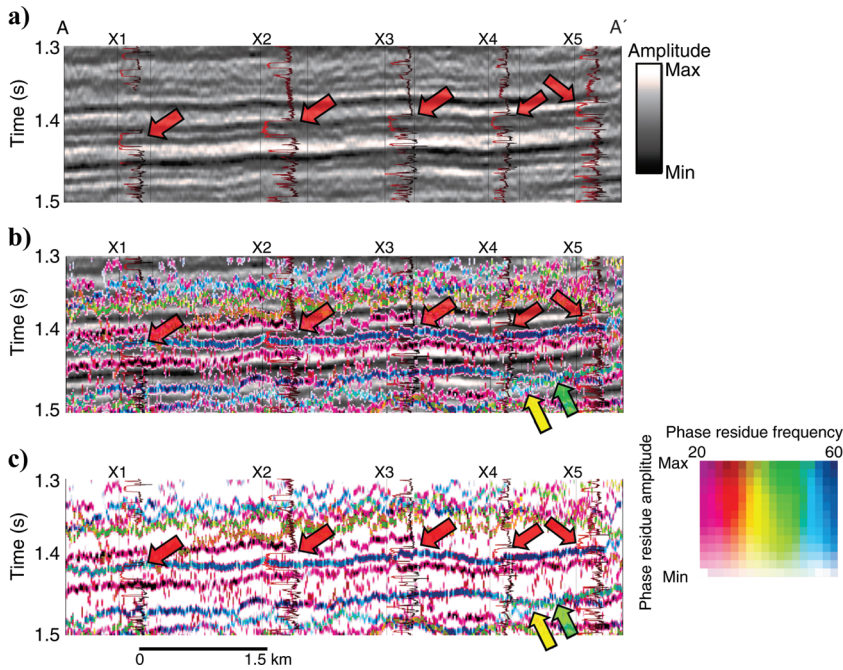


Figure 11. Vertical section AA' through (a) seismic amplitude data, (b) seismic amplitude data corendered with CWT phase residue attributes using a 2D color map (Guo et al., 2008), and (c) CWT phase-residue attributes using a 2D color map (Guo et al., 2008). Red arrows indicate the base of a GR sequence. Yellow arrows indicate a channel feature in the CWT phase-residue attributes that is masked in the seismic data. The green arrows are interpreted as the levee of the channel interpreted by the yellow arrow or an adjacent channel that is not resolved in the seismic section. In (c), the sand body reflection interface is better resolved in the phase-residue attribute; notice the channel features (green and yellow arrows).

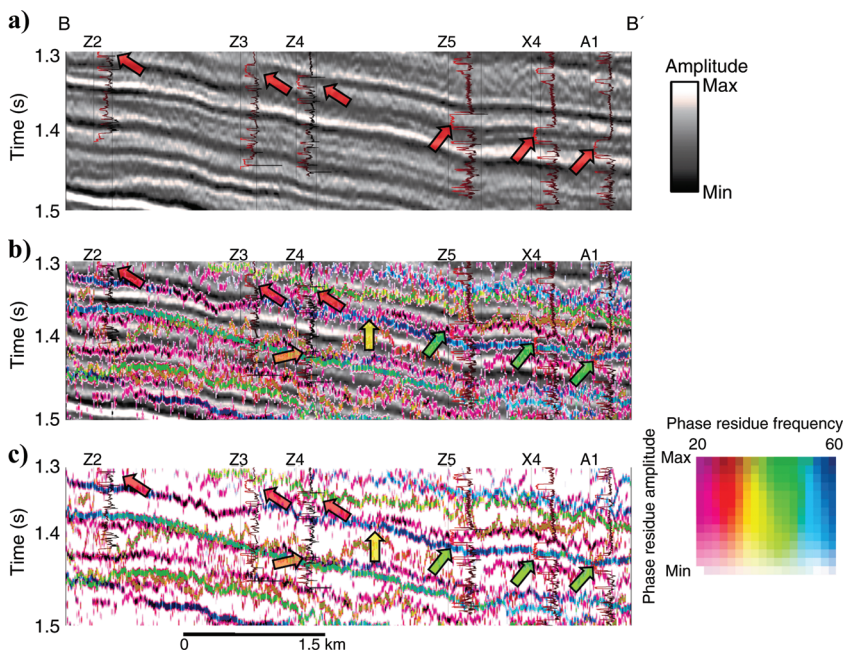


Figure 12. (a) Vertical section BB' through seismic amplitude data, (b) seismic amplitude data corendered with CWT phase residue attributes using a 2D color map (Guo et al., 2008), and (c) CWT phase-residue attributes using a 2D color map (Guo et al., 2008). Red arrows indicate a continuous sand body following the gamma-ray-log response and the seismic amplitude data. With the aid of the attribute, the continuous sand body in (a) is reinterpreted as two different sand bodies at different structural levels (red and green arrows). The yellow arrows indicate a feature we interpret to be a pinch-out of the lower sand body. The lower sand body is better delineated by the time-phase-residue attribute (c). Orange arrow indicates a channel feature that correlates with a coarsening-upward sequence in the gamma-ray log of well Z4. This feature is also identified on Figures 14, 15, and 16b.

16b) show lineaments that overlap; they may be related to changes in depositional environments (e.g., channel system to flood plains). However, beyond the three main features

detected by coherence (red arrows), several channel features are also identified (green arrows) with the help of phase-residue attributes.

Figure 13. (a) Vertical section CC' through the seismic amplitude data, (b) seismic amplitude data corendered with CWT phase-residue attributes using a 2D color map (Guo et al., 2008), and (c) CWT phase-residue attributes using a 2D color map (Guo et al., 2008). Red arrows indicate similar gamma-ray-log responses for wells Y2, Z3, and Jay Jay 2. Notice the change in character of the seismic amplitude data going from well Y2 to the Jay Jay 2 well in (a). With the aid of the attribute, the continuous gamma-ray responses in (a) are reinterpreted to be three different sand bodies at different structural levels (red, green, and yellow arrows); blue arrows indicate the pinch-out in the lower and upper sand bodies. The pinch-out of the sands can be seen in the attribute section (c) but cannot be seen in seismic amplitude section because of tuning effects. In addition, the channel features highlighted by the yellow and green arrows are best defined by the phase-residue attribute.

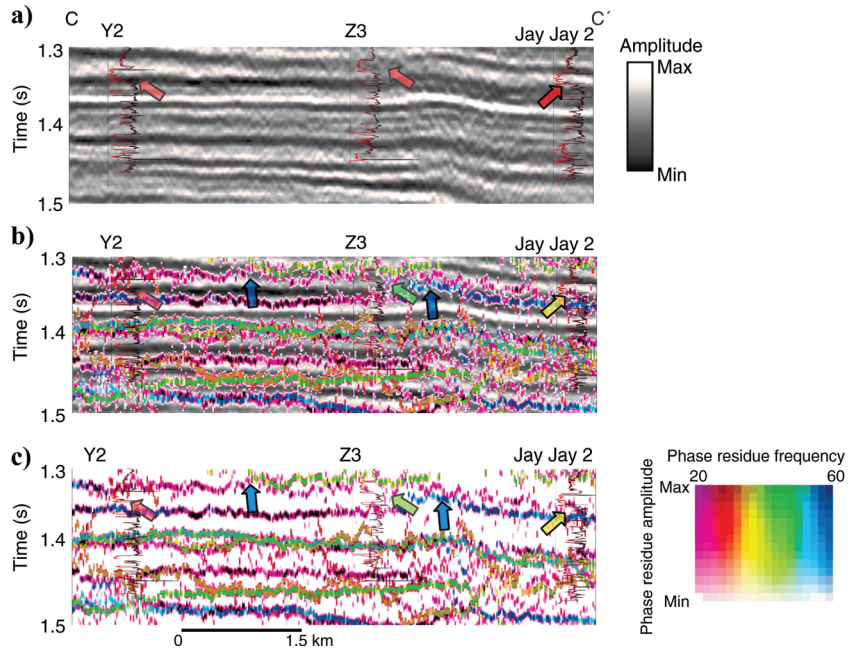
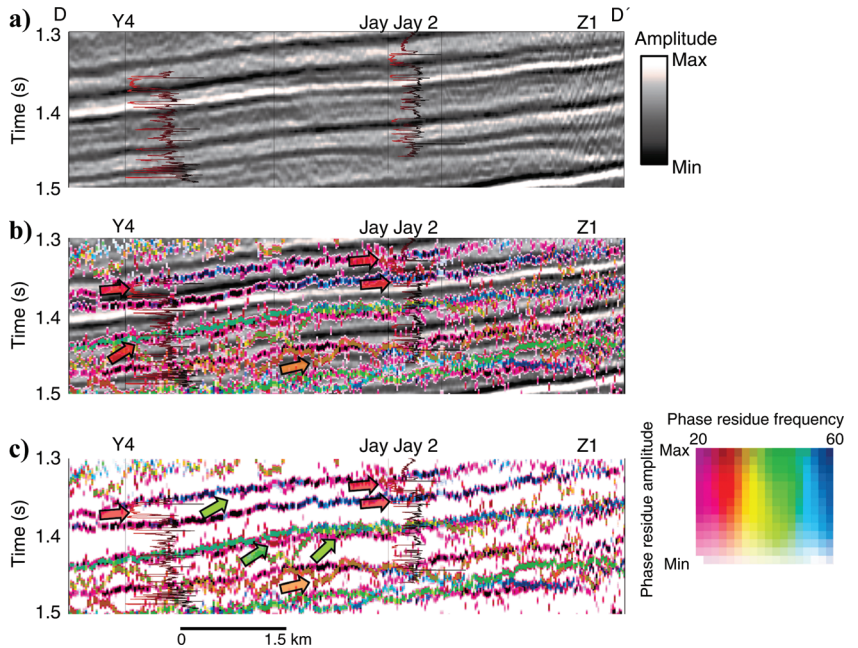


Figure 14. (a) Vertical section DD' through the seismic amplitude data, (b) seismic amplitude data corendered with CWT phase-residue attributes using a 2D color map (Guo et al., 2008), and (c) CWT phase residue attributes using a 2D color map (Guo et al., 2008). In this section, no distinctive features are imaged in the seismic data, probably because of seismic resolution. Peyton et al. (1998) refer to well Jay Jay 2 in their work and state that this well produces from approximately 15 m (50 ft) of sand and that no channels were imaged in the area near the well. Channel features are found at different stratigraphic levels, indicated by the red arrows in wells Jay Jay 2 and Y4. Orange arrow indicates the channel feature identified in Figure 12. (c) Some other channel features are identified in the phase-residue section (green arrows).



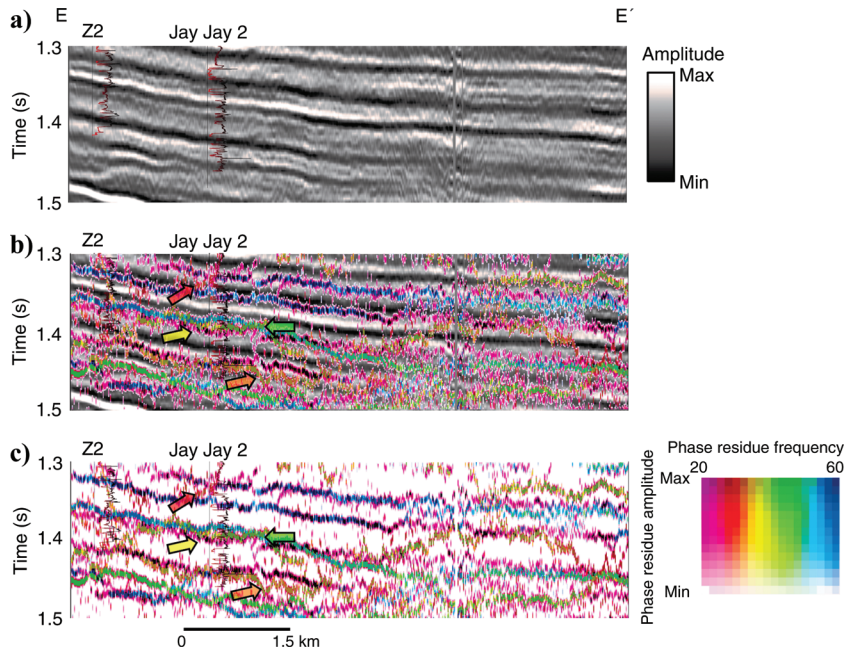


Figure 15. (a) Vertical section EE' through seismic amplitude data, (b) seismic amplitude data corendered with CWT phase-residue attributes using a 2D color map (Guo et al., 2008), and (c) CWT phase-residue attributes using a 2D color map (Guo et al., 2008). As in Figure 11, channel features are detected by the phase-residue attributes (red and yellow arrows). The lower channel feature has a different response in the residual peak amplitude attribute that correlates with the boundary between a low and a high response in the gamma-ray curve (green arrow). Orange arrows indicate the channel feature identified in Figure 12.

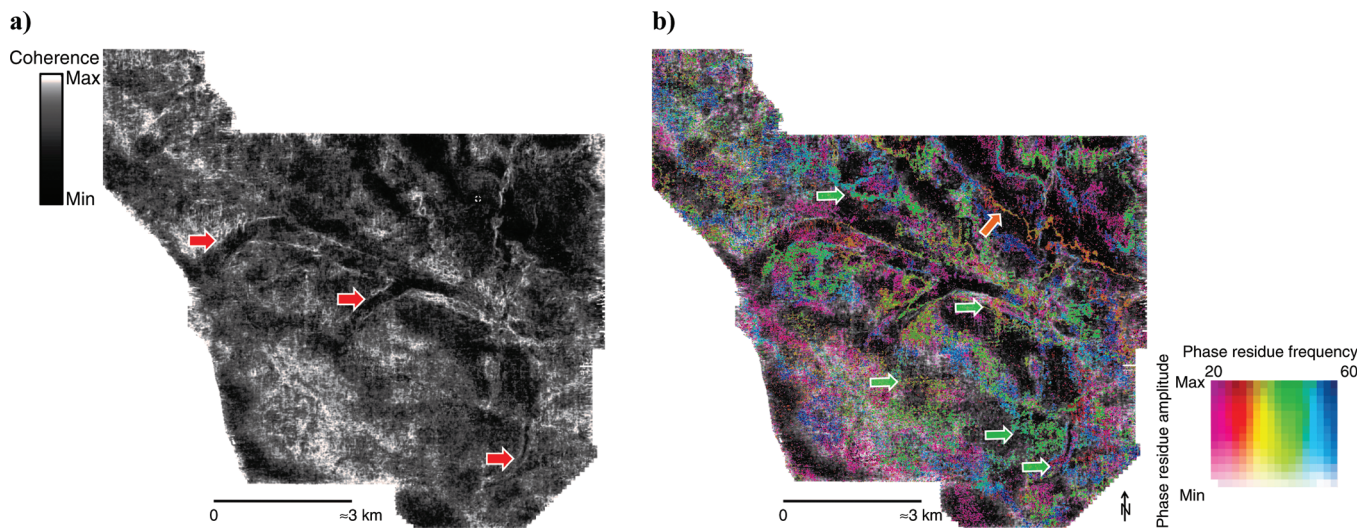


Figure 16. (a) Phantom horizon slice 80 ms below the Skinner horizon through the coherence volume, computed using a 9-trace, ± 20 -ms analysis window. Three incised channels are identified (red arrows). (b) Phase-residue amplitude and frequency attributes blended using a 2D color map (Guo et al., 2008) 80 ms below the Skinner horizon, corendered with energy-ratio similarity. In addition to the features identified in Figure 16a, several channel features are identified (green and orange arrows).

CONCLUSIONS

We have shown how phase residues introduced in signal processing can be applied to Morlet CWT time-frequency distributions generated by spectral decomposition. CWT phase residues are related to transitions between different phase values. Although they are not a thin-bed detection tool, they do reveal important stratigraphic features. Through calibration using 15 wells and a 350-km² seismic survey, our interpretation indicates these phase residues appear to be sensitive to subtle discontinuities that are not easily seen in input seismic amplitude data. We believe phase attributes are sensitive to the same kinds of stratigraphic discontinuities seen by analyzing the magnitude

component of time-frequency distribution using wavelet transforms and the continuous wavelet transform. Because phase is often a more robust seismic measure than magnitude, it holds significant promise in mapping stratigraphic unconformities.

ACKNOWLEDGMENTS

The authors thank Danilo Velis, Mauricio Sacchi, Oleg Portniaguine, and two anonymous referees whose careful reviews and detailed comments helped improve the readability of this paper. The authors also thank Chesapeake for providing the data used in this study and permission to publish this work, as well as the industry

sponsors of the University of Oklahoma Attribute-Assisted Seismic Processing and Interpretation (AASPI) Consortium.

REFERENCES

- Bone, D. J., 1991, Fourier fringe analysis: The two-dimensional phase unwrapping problem: *Applied Optics*, **30**, 3627–3632, doi:10.1364/AO.30.003627.
- Castagna, J., S. Sun, and R. Siegfried, 2003, Instantaneous spectral analysis: Detection of low-frequency shadows associated with hydrocarbons: *The Leading Edge*, **22**, 120–127, doi:10.1190/1.1559038.
- Ghiglia, D., and M. D. Pritt, 1998, *Two-dimensional phase unwrapping: Theory, algorithms, and software*: Wiley-Interscience.
- Guo, H., S. Lewis, and K. J. Marfurt, 2008, Mapping multiple attributes to three- and four-component color models — A tutorial: *Geophysics*, **73**, no. 3, W7–W19, doi:10.1190/1.2903819.
- Hall, M., and E. Trouillot, 2004, Predicting stratigraphy with spectral decomposition: Annual National Convention, Canadian Society of Exploration Geophysicists, Conference Abstracts, http://www.cseg.ca/conventions/abstracts/2004/2004abstracts_046S0131-Hall-M-Preicting_strat.pdf, accessed 12 November 2010.
- Hart, B., 2008, Stratigraphically significant attributes: *The Leading Edge*, **27**, 320–324, doi:10.1190/1.2896621.
- Henry, S., 2004, Understanding seismic amplitudes: Search and Discovery article 40135, adapted from AAPG Explorer Geophysical Corner, July/August, <http://www.searchanddiscovery.net/documents/2004/henry/images/henry.pdf>, accessed August 10, 2009.
- Holschneider, M., 1995, *Wavelets: An analysis tool*: Oxford University Press.
- Itoh, K., 1982, Analysis of the phase unwrapping algorithm: *Applied Optics*, **21**, no. 14, 2470, doi:10.1364/AO.21.002470.
- Kaplan, S. T., and T. Ulrych, 2007, Phase unwrapping: A review of methods and a novel technique: National Convention, Canadian Society of Exploration Geophysicists, Conference Abstracts, 534–537.
- Léonard, F., 2007, Phase spectrogram and frequency spectrogram as new diagnostic tools: *Mechanical Systems and Signal Processing*, **21**, no. 1, 125–137, doi:10.1016/j.ymssp.2005.08.011.
- Liu, J., and K. Marfurt, 2007, Instantaneous spectral attributes to detect channels: *Geophysics*, **72**, no. 2, P23–P31, doi:10.1190/1.2428268.
- Matos, M. C., P. L. M. Osorio, and P. R. S. Johann, 2007, Unsupervised seismic facies analysis using wavelet transform and self-organizing maps: *Geophysics*, **72**, no. 1, P9–P21, doi:10.1190/1.2392789.
- Matos, M. C., P. L. M. Osorio, E. C. Mundim, and M. A. S. Moraes, 2005, Characterization of thin beds through joint time-frequency analysis applied to a turbidite reservoir in Campos basin, Brazil: 75th Annual International Meeting, SEG, Expanded Abstracts, 1429–1432, doi:10.1190/1.2147957.
- Matos, M. C., K. Zhang, K. J. Marfurt, and R. Slatt, 2009, Stratigraphic discontinuities mapped through joint time-frequency seismic phase unwrapping: 79th Annual International Meeting, SEG, Expanded Abstracts, 1087–1091, doi:10.1190/1.3513124.
- Partyka, G., J. Gridley, and J. Lopez, 1999, Interpretational applications of spectral decomposition in reservoir characterization: *The Leading Edge*, **18**, 353–360, doi:10.1190/1.1438295.
- Peyton, L., R. Bottjer, and G. Partyka, 1998, Interpretation of incised valleys using new 3-D seismic techniques: A case history using spectral decomposition and coherency: *The Leading Edge*, **17**, 1294–1298, doi:10.1190/1.1438127.
- Roden, R., and H. Sepulveda, 1999, The significance of phase to the interpreter: Practical guidelines for phase analysis: *The Leading Edge*, **18**, 774–777, doi:10.1190/1.1438375.
- Shatilo, A. P., 1992, Seismic phase unwrapping: Methods, results, problems: *Geophysical Prospecting*, **40**, no. 2, 211–225, doi:10.1111/j.1365-2478.1992.tb00372.x.
- Stark, T., 2003, Unwrapping instantaneous phase to generate a relative geologic time volume: 73rd Annual International Meeting, SEG, Expanded Abstracts, 1707–1710.
- Suarez, Y., K. J. Marfurt, and M. Falk, 2008, Seismic attribute-assisted interpretation of channel geometries and infill lithology: A case study of Anadarko basin Red Fork channels: 78th Annual International Meeting, SEG, Expanded Abstracts, 963–967.
- Taner, M. T., F. Koehler, and R. E. Sheriff, 1979, Complex seismic trace analysis: *Geophysics*, **44**, 1041–1063, doi:10.1190/1.1440994.
- Widess, M. B., 1973, How thin is a thin bed?: *Geophysics*, **38**, 1176–1180, doi:10.1190/1.1440403.